Effects of different back contacts on photovoltaic performances of CdTe/CdS thin film solar cells

SAIME SEBNEM CETIN AYDIN[a, b, c,*]
[a]*Gazi University, Faculty of Applied Sciences, Department of Photonics, Ankara, Turkey*
[b]*Gazi University, Photonics Application and Research Center, Ankara, Turkey*
[c]*Gazi University, Faculty of Sciences, Department of Physics, Ankara, Turkey*

The CdTe/CdS thin film solar cell structure was deposited on the fluorine tin oxide (FTO) coated glass substrate using radio frequency (RF) magnetron sputtering system. CdTe/CdS thin film solar cells were produced using back metal contacts (Pt, Ni, Au, and Ag) with different work functions. The structural properties of the thin film were analyzed by X-ray Diffraction (XRD) method. For all solar cells, the fundamental solar cell parameters such as short circuit current (I_{SC}), open-circuit voltage (V_{OC}), fill factor (*FF*), and energy conversion efficiency (η) were determined from current-voltage (*I–V*) characteristics in the dark and under AM1.5G (100 mW/cm^2).

(Received September 21, 2020; accepted April 8, 2021)

Keywords: CdTe/CdS solar cell, Back contact metal, Solar cell parameters, *I-V* characteristics

1. Introduction

Because of the rising energy demand, energy consumption will be 30 TW by 2050 for the sustainable development of the world. The distance travelled by countries in their sustainable progress is directly proportional to their energy production rates [1, 2]. Such a consumption forecast draws attention to the importance of using low cost, abundant and clean energy resources that do not contain fossil fuels. Here, the use of renewable energy resources will meet the energy demand and characteristics needed. Especially the most important way of this is to convert the photon energy from the sun directly into electrical energy through the solar cell [3-6].

Cadmium Telluride (CdTe) has a direct optical bandgap of 1.45 eV, which is the optimum bandgap value for solar cells. It is a highly preferred material for solar cell technology owing to its high photovoltaic conversion efficiency, cost-effectiveness, thermal cell stability, long-term stable performance, and clean generation of solar electricity [7-9].

CdTe based material systems are favored in a CdS/CdTe heterojunction systems because of the high optical absorption coefficient of over 5×10^5 cm^{-1}, so all the potential photons of greater energy than the bandgap can be absorbed within an ultra-very thin CdTe absorber layer. Besides, as a suitable window layer, CdS with n-type is the best suitable material with the p-CdTe absorber. CdS affect the cell's conversion efficiency, where thinner CdS films build higher short circuit current densities [10].

Heterojunction CdS/CdTe based solar cells can be accumulated by the carrying out different low-cost techniques such as chemical bath deposition (CBD), physical vapour deposition (PVD), close-spaced-sublimation (CSS) and magnetron sputtering. Among these methods, the magnetron sputtering is widely used and advantageous due to its ability to get a uniform, dense, and exact stoichiometric thin films [11-20].

In the last 20 years, the efficiency of CdS/CdTe based solar cells has been increased by 1.5% in laboratory conditions. 20.4% cell efficiency and 13.9% module efficiency have been achieved by First Solar Research Group [6, 8, 21, 22]. The most important of main and significant challenges for the high efficient and stable CdS/CdTe based solar cell is the p-CdTe with back contact metal. The back metal contact has a configuration of stable and low resistance. At first, heterojunction CdS/CdTe solar cells exhibit good efficiencies; however, the efficiency was decreased in the long run. Since metals used as back contact, they diffuse into the cell over time and degrade cell efficiency. To deal with this problem in the heterojunction CdS/CdTe solar cells, Back Surface Field (BSF) layer produced by higher bandgap material (i.e., ZnTe or CdZnTe) is added to between the CdS/CdTe absorbent layer and the metal contact [2].

Using of BSF layer showed itself in solar cell applications, especially in the eighties [23]. In solar cells designed with BSF technique, an effective surface area is created, and cell output parameters can be improved. The BSF layer surrounds the photo-formed carriers around the p-n junction and allows it to be better collected by the internal electric field.

In this study, the structural properties of CdTe/CdS thin film solar cell structure were investigated. The phase and crystal quality of each layer were determined by XRD measurement. Different metals were used in the metallization process to increase the efficiency of the solar cell. Fundamental device parameters of the solar cell structure such as short circuit current (I_{SC}), open-circuit voltage (V_{OC}), fill factor (*FF*), and energy conversion

efficiency (η) were extracted from the current-voltage (*I-V*) characteristics.

2. Experimental details

The CdTe/CdS solar cell structure was coated on the FTO coated glass substrate. The schematic diagram of the thin film solar cell was shown in Fig. 1. NANOVAK NVTS-500 Sputtering System was used to realize solar cell structure. High purity (99.999%) ZnO, CdS, CdTe, and ZnTe targets were used for the thin film layers coating. FTO coated glass, which was supplied clean enough, was cleaned again with dry nitrogen before loading into the sputtering system. The base pressure of the sputtering system before the coating is in the order of 10^{-6} *Torr*. The coatings of the layers forming the sample were carried out at a constant pressure of 20 *mTorr*. Other coating parameters were given in Table 1.

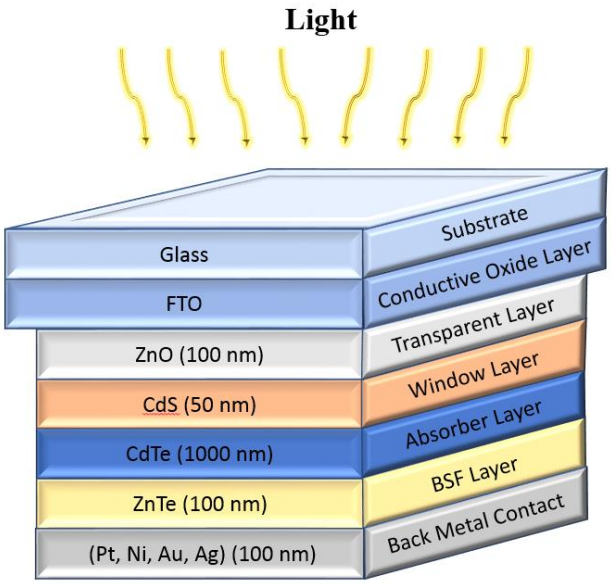

Fig. 1. The schematic diagram of the thin film solar cell (color online)

Table 1. Coating parameters of thin film solar cell

	Solar Cell Structure			
Layer Name	ZnO	CdS	CdTe	ZnTe
Coating Pressure (*mTorr*)	20			
Substrate Temperature (°C)	Room Temp.			
Sputter Power (*Watt*)	150	100	30	30
Coating Time (*minutes*)	20	5	300	30
Thickness of Layer (*nm*)	100	50	1000	100

X-ray Diffractometer System (XRD) at Gazi University Photonics Application and Research Center was used to determine the structural properties of the sample. After the structural analyzes were completed, the metal contacts of solar cells were fabricated with Bestec Thermal Evaporation System using four different metals (Pt, Ni, Au, Ag) with 100 *nm* thickness. Fabrication geometry was created so that the active areas of the cells were 1 *cm* × 1 *cm*. Then, the basic parameters of solar cells were determined using Keithley 4200 Sourcemeter and Oriel Sol1A Class AAA Solar Simulator in the dark and under AM1.5G (100 mW/cm^2).

3. Results and discussion

The XRD pattern of the thin film solar cell was represented in Fig. 2. As seen in Fig. 2, the peaks observed at 24.04°, 26.46°, 28.46°, and 34.46° are the diffraction peaks arising from the cubic phase of CdTe at (111) plane, the cubic phase of CdS at (111) plane, the cubic phase of ZnTe at (200) plane, and the hexagonal phase of ZnO at (002) plane, respectively (JCPDS file No. 75-2086, 80-0019, 15-0746, 79-2205). As a result of the coating, it is concluded that the layers are formed in the structure, and the crystal quality is good.

The particle size (*D*) of the film is calculated using Scherrer's formula [24, 25]

$$D = \frac{k\lambda}{B\cos\theta} \quad (1)$$

where k = 0.9 is Scherrer's constant, λ =1.540598 Å is the wavelength of X-ray, B is full-width at half maximum (FWHM in radians) of the diffraction peak, and θ is Bragg's angle. The particle sizes in CdTe, CdS, ZnTe, and ZnO films are of the order 40.6 *nm*, 25.9 *nm*, 24.6 *nm*, and 34.8 *nm*, respectively. These values are in good agreement with the reported ones [26-30].

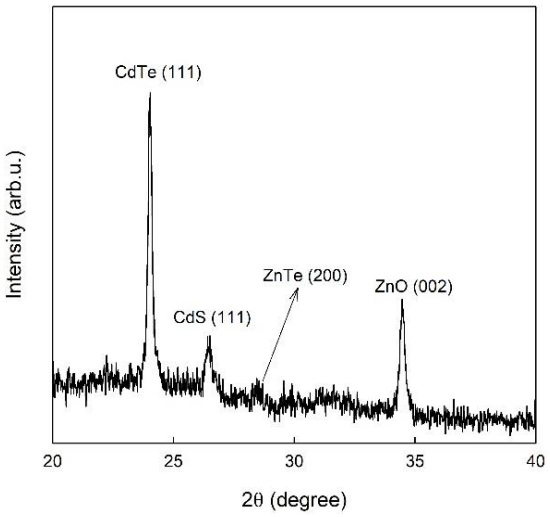

Fig. 2. XRD pattern of the thin film solar cell

I-V curves under dark and illumination of solar cell structures for different back metal contacts (Pt, Au, Ni, Ag) were represented in Fig. 3. Since the CdTe layer has a porous structure, the metallization material used as a back

contact in the solar cell structure generally leaks into the structure, and the cell does not work. The ZnTe BSF layer used in this study prevents the metal from leaking into the structure. As seen in Table 2, the decrease in the metal's work function creates a reduction in efficiency.

Table 2 shows the change of fundamental solar cell parameters depending on the work function of the metal used. Efficiency (η) values were calculated using equation $\eta=P_{out} / P_{in} =(I_{SC} \times V_{OC} \times FF) / P_{in}$, where V_{OC} open-circuit voltage, I_{SC} short circuit current, FF fill factor, and P_{in} the intensity of the incident light [4]. η values were found as 11.43%, 11.06%, 10.87%, and 9.90% for Pt, Ni, Au, and Ag back metal contacts, respectively. As seen from Table 2, as the work function of the metal increases, a slight increasing is seen in the solar cell efficiency. In literature, there are studies on efficiency analysis related to the work function of metal in CdTe solar cells [31, 32]. Anwar et al. [31] and Haddout et al. [32] reported that the efficiency value of the CdTe-based solar cell increased with the increase in the working function of the back metal contact.

To increase the efficiency of solar cells, it is necessary to study on different metal that can form suitable metal-semiconductor junctions. In literature, as expressed in the introduction, there are studies on the efficiency increase of CdTe based solar cells. Among these studies, Özen [6] achieved 10.39% efficiency by applying Au as back contact in the CdTe based solar cell containing BSF and Distributed Bragg Reflector (DBR) layers. In the presented study, 11.06% efficiency was reached using Au in the solar cell structure without DBR layer. Also, the efficiency of 11.43% was achieved by working Pt as a back contact, which has a higher work function than Au. When the efficiency value of the cells obtained by using Au and Pt metals was compared, it was observed that there was an increase of approximately 3.2% in the efficiency value when Pt metal was used as the back contact. In light of these results, it is observed a slight increase in the efficiency value with the increase in the work function of the metal used as back contact due to metal semiconductor interface state effect. These results will be useful data for future studies.

Table 2. Output parameters of thin film solar cells with different contact materials

Contact Material	***Work Function (eV)***	***I_{SC} (mA)***	***V_{OC} (V)***	***FF (%)***	***η (%)***
Pt	5.64 [33-35]	15.41	0.9595	77	11.43
Au	5.47 [33-35]	15.17	0.9585	76	11.06
Ni	5.22 [33-35]	15.35	0.9225	77	10.87
Ag	4.64 [33-35]	13.97	0.9295	76	9.90

4. Conclusion

The CdTe based solar cell structure containing ZnTe BSF layer was deposited on FTO coated glass with RF sputter system.

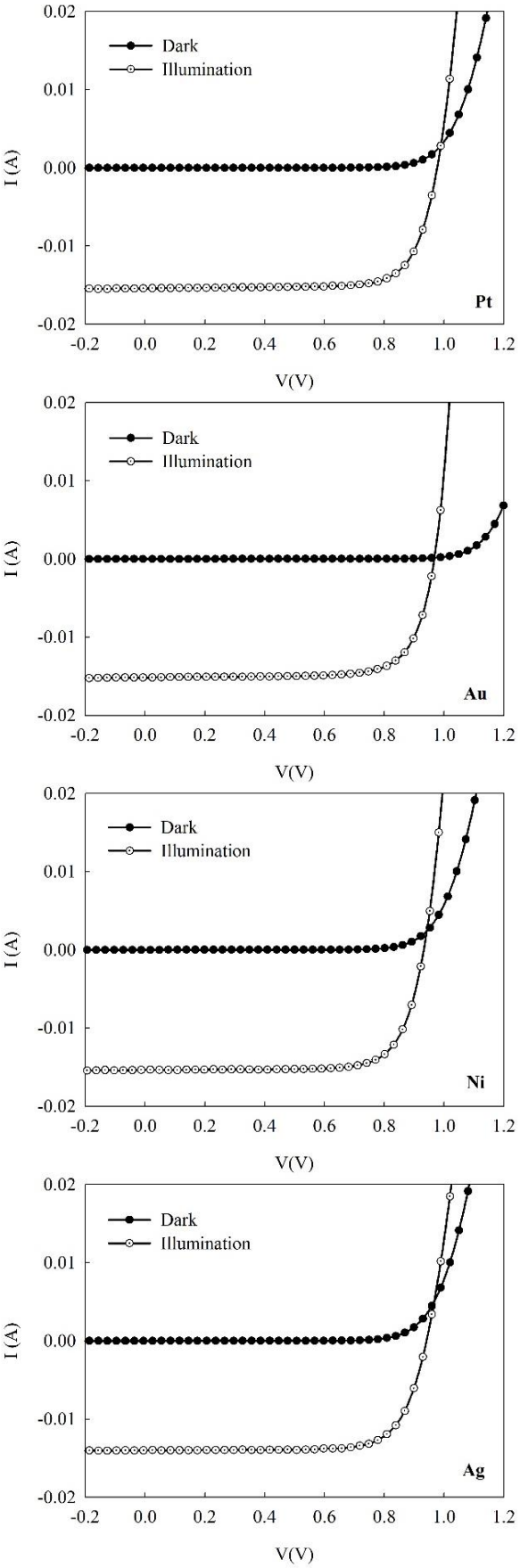

Fig. 3. The current-voltage (I-V) characteristic of the samples at room temperature in the dark and under AM1.5G (100 mW/cm^2)

The phases of the layers and the crystal quality of the structure were determined by XRD. Pt, Ni, Au, and Ag metals with different work functions were used as back contacts. The values of I_{SC} were found as 15.41 mA, 15.17 mA, 15.35 mA, and 13.97 mA for Pt, Ni, Au, and Ag back metal contacts, respectively. The values of V_{OC} were found as 0.9595 V, 0.9585 V, 0.9225 V and 0.9295 V for Pt, Ni, Au, and Ag back metal contacts, respectively. The values of *FF* were found as 77%, 76%, 77%, and 76% for Pt, Ni, Au and Ag back metal contacts, respectively. η values were found as 11.43%, 11.06%, 10.87%, and 9.90% for Pt, Ni, Au, and Ag back metal contacts, respectively. Experimental results showed an increasing in solar cell efficiency due to the increased work function.

Acknowledgements

This work was supported by Gazi University Scientific Research Projects Unit [Grant Number: 05/2017-20] and The Republic of Turkey Presidency of Strategy and Budget [Grants Numbers: 2011K120290 and 2016K121220].

References

[1] R. Mendoza-Perez, J. Sastre-Hernandez, G. Contreras-Puente, O. Vigil-Galan, Sol. Energy Mater. Sol. Cells **93**(1), 79 (2009).
[2] M. Dey, M. Dey, M. Matin, N. Amin, 9th International Conference on Electrical and Computer Engineering (ICECE), 590 (2016).
[3] B. Kınacı, Y. Özen, T. Asar, S. S. Cetin, T. Memmedli, M. Kasap, S. Özçelik, J. Mater. Sci. Mater. Electron. **24**(9), 3269 (2013).
[4] Y. Özen, N. Akin, B. Kinaci, S. Özçelik, Sol. Energy Mater. Sol. Cells **137**, 1 (2015).
[5] A. Muhammetgulyyev, B. Kinaci, A. Aho, Y. Yalcin, C. Cetinkaya, F. Kuruoglu, M. Guina, A. Erol, Appl. Phys. A **125**, 27 (2019).
[6] Y. Özen, Appl. Phys. A, **126**, 632 (2020).
[7] D. L. Bätzner, A. Romeo, H. Zogg, R. Wendt, A. N. Tiwari, Thin Solid Films **387**(1-2), 151 (2001).
[8] T. Aramoto, S. Kumazawa, H. Higuchi, T. Arita, S. Shibutani, T. Nishio, J. Nakajima, M. Tsuji, A. Hanafusa, T. Hibino, Jpn. J. Appl. Phys. **36**(10), 6304 (1997).
[9] E. Colegrove, R. Banai, C. Blissett, C. Buurma, J. Ellsworth, M. Morley, S. Barnes, C. Gilmore, J. D. Bergeson, R. Dhere, M. Scott, T. Gessert, S. Sivananthan, J. Electron. Mater. **41**(10), 2833 (2012).
[10] V. Krishnakumar, J. Han, A. Klein, W. Jaegermann, Thin Solid Films **519**(21), 7138 (2011).
[11] B. Kinaci, T. Asar, Y. Ozen, S. Ozcelik, Optoelectron. Adv. Mat. **5**(4), 434 (2011).
[12] B. Kinaci, T. Asar, S.S. Cetin, Y. Ozen, K. Kızılkaya, J. Optoelectron. Adv. M. **14**(11-12), 959 (2012).
[13] N. Akin, U. Ceren Baskose, B. Kinaci, M. Cakmak, S. Ozcelik, Appl. Phys. A **119**(3), 965 (2015).
[14] B. Kinaci, S. Özçelik, J. Electron. Mater. **42**(6), 1108 (2013).
[15] I. Kars, S. S. Cetin, B. Kinaci, B. Sarikavak, A. Bengi, H. Altuntaş, M. K. Öztürk, S. Özçelik, Surf. Interface Anal. **42**(6-7), 1247 (2010).
[16] N. Akin, B. Kinaci, Y. Ozen, S. Ozcelik, J. Mater. Sci. Mater. Electron. **28**(10), 7376 (2017).
[17] B. Kinaci, N. Akin, I. Kars Durukan, T. Memmedli, S. Özçelik, Superlattices Microstruct. **76**, 234 (2014).
[18] B. Kınacı, Ç. Çetinkaya, E. Çokduygulular, H. I. Efkere, N. Akin Sönmez, S. Özçelik, J. Mater. Sci.: Mater. Electron. **31**, 8718 (2020).
[19] E. Çokduygulular, Ç. Çetinkaya, Y. Yalçin, B. Kinaci, J. Mater. Sci.: Mater. Electron. **31**, 13646 (2020).
[20] F. Güzelçimen, B. Tanören, Ç. Çetinkaya, M. Dönmez Kaya, H. I. Efkere, Y. Özen, D. Bingöl, M. Sirkeci, B. Kınacı, M. B. Ünlü, S. Özçelik, Vacuum. **182**, 109766 (2020).
[21] S. Khosroabadi, S. H. Keshmiri, S. Marjani, J. Eur. Opt. Soc. **9**, 1 (2014).
[22] T. M. Razykov, C. S. Ferekides, D. Morel, E. Stefanakos, H. S. Ullal, H. M. Upadhyaya, Sol. Energy **85**(8), 1580 (2011).
[23] M. A. Islam, Y. Sulaiman, N. Amin, Chalcogenide Lett. **8**(2), 65 (2011).
[24] S. S. Cetin, S. Corekci, M. Cakmak, S. Ozcelik, Cryst. Res. Tech. **46**(11), 1207 (2011).
[25] K. N. Nithyayini, Sheela K. Ramasesha, Metall. Mater. Trans. E **2**, 157 (2015).
[26] K.S. Rahman, M.N. Harif, H.N. Rosly, M. I. B. Kamaruzzaman, Md. Akhtaruzzaman, M. Alghoul, H. Misran, N. Amin, Results Phys. **14**, 102371 (2019).
[27] A. Ashok, G. Regmi, A. Romero-Núñez, M. Solis-López, S. Velumani, H. Castaneda, J. Mater. Sci.: Mater. Electron. **31**, 7499 (2020).
[28] G. K. Rao, K. V. Bangera, G. K. Shivakumar, Mater. Res. Bull. **45**(10), 1357 (2010).
[29] S. Chander, M.S. Dhaka, Results Phys. **8**, 1131 (2018).
[30] T. P. Rao, M. C. Santhoshkumar, App. Surf. Sci. **255**(8), 4579 (2009).
[31] F. Anwar, S. Afrin, S. S. Satter, R. Mahbub, S. M. Ullah, Int. J. Renew. Energy Res. **7**(2), 885 (2017).
[32] A. Haddout, A. Raidou, M. Fahoume, Optoelectron. Lett. **14**(2), 98 (2018).
[33] J. Holzl, F. K. Schulte, Work Functions of Metals, in Solid Surface Physics, Springer-Verlag, Berlin, 1979.
[34] J. C. Riviere, Work Function: Measurements and Results, in Solid State Surface Science, **1**, Decker, New York, 1969.
[35] H. B. Michaelson, J. Appl. Phys. **48**, 4729 (1977).

*Corresponding author: cetins@gazi.edu.tr